

Oxidation of CO Catalyzed by a Cu Cluster: Influence of an Electric Field

Wei Liu,^[a, b] Yonghao Zhao,^[b] Renqin Zhang,^[a] Ying Li,^[b] Enrique J. Lavernia,^{*[b]} and Qing Jiang^{*[a]}

Adsorption ability and reaction rate are two essential parameters that define the efficiency of a catalyst. Herein, we implement density functional theory (DFT) and report that CO can be oxidized by a pyramidal Cu cluster with an associated reaction barrier $E_b = 1.317$ eV. In this case, our transition state calculations reveal that the barrier can be significantly lowered after superimposing a negative electric field. Moreover, when the field intensity corresponds to $F = -0.010$ au, the magnitude of

$E_b = 0.698$ eV is equivalent to—or lower than—those of typical catalysts such as Pt, Rh, and Pd. The superimposition of a positive field is found to enhance the release of the nascent CO₂ molecule. Our study demonstrates that small Cu clusters have better adsorption ability than the corresponding flat surface while the field can be used to enhance the purification of the exhaust gas.

1. Introduction

The oxidation behavior of CO on metal surfaces is of interest given the relevance to fuel combustion and corresponding purification of automotive exhaust.^[1–5] In addition to the obvious practical implications, there remain some fundamental questions in this system, such as the preferable adsorption sites for the CO/Pt(111) surface,^[6–9] and the prominent active sites for CO oxidation on the RuO₂(110) surface.^[10–11] Several new computational methodologies, including the relativistic correction,^[12–15] the periodic hybrid density functional theory (DFT),^[7, 16–17] and the DFT+U approach,^[8, 18–21] have been proposed to provide insight into these fundamental questions. Therefore, the oxidation of CO has been recognized as a prototype for the study of gas/surface interactions and heterogeneous catalysis.^[22–24] Gas adsorption is apparently the most essential and the very first step in the catalytic oxidation reaction. In fact, a stronger binding strength between the adsorbates and the catalyst may promote associated product formation.^[25–28] The binding strength can be described by the adsorption energy, E_{adr} , which is defined as the energy difference between the adsorption system with the individual metallic surface and gas-phase molecules. To effectively convert CO to CO₂ at low temperatures, oxidation of CO on the late transition metals (especially the three-way catalysts composed of Rh, Pt, and Pd) is widely viewed as an effective approach.^[14, 24, 29–30]

In addition to E_{adr} , the energy barrier E_b is another essential parameter to describe the rate of a reaction. Earlier attempts, both experimentally^[23, 25, 31–34] and theoretically,^[25, 35–39] have been made to lower the E_b values for CO oxidation on metallic surfaces. In contrast, recent studies address novel catalysts such as alloys,^[40–42] clusters,^[1, 40, 43–45] and even metallic nanotubes.^[46] Among them, An et al.^[46] reported that the CO oxidation catalyzed by a helical Au(5,3) nanotube is likely to occur at room temperature. The high catalytic activity of Au nanotubes was attributed to the partial charge transfer and the electronic resonance among the d states of Au atoms and the

antibonding $2\pi^*$ states of C-O and O-O. By synthesizing the highly dispersed Au-Cu alloy nanoparticles, Liu et al.^[42] demonstrated that this alloy surface exhibited superior performance compared with the monometallic particles in catalyzing CO oxidation. The presence of Cu modifies the charge distribution of Au and thereby contributes much to the activation of O.

From the above discussions, one may hypothesize that small particles (with a diameter ranging 1–10 nm) are likely to have larger binding strength than their corresponding bulk flat surfaces, which is induced by profoundly different electronic structures due to the difference in coordination number of the surface atoms. In addition, the catalytic activity can be further enhanced if the charge transfer between an adsorbate and metal is enhanced. In our recent works, a series of pyramidal Cu clusters were simulated to study the size-dependent cohesive energy E_c and adsorption properties.^[47–48] Therefore, a pyramidal Cu cluster in the present work is still employed as a *prototype system* to look into the oxidation behavior of CO molecules. Inspection of the published literature implies that most prior studies were centered on the adsorption properties for CO/Cu systems.^[49–54] Although several works have discussed the reaction process of CO on the Cu surfaces,^[55–56] oxidation of CO catalyzed by a Cu cluster has not been reported up to now, to the best of our knowledge. In addition, we investigate the influence of a superimposed electric field on this reaction.

[a] W. Liu, R. Q. Zhang, Prof. Q. Jiang

Key Laboratory of Automobile Materials, Ministry of Education and School of Materials Science and Engineering
Jilin University, Changchun 130022 (China)
Fax: (+86) 431-85095876
E-mail: jiangq@jlu.edu.cn

[b] W. Liu, Dr. Y. H. Zhao, Dr. Y. Li, Prof. E. J. Lavernia

Department of Chemical Engineering and Materials Science
University of California, Davis, CA 95616 (USA)
Fax: (+1) 530-752-8058
E-mail: lavernia@ucdavis.edu

The rationale for this strategy is based on recent studies on the influence of an electric field on adsorption.^[57–59] It is worth noting that study of an oxidation reaction in the presence of an electric field has heretofore never been reported. The current study aims to provide insight into two fundamental questions: i) What is the possible catalytic pathway for CO oxidation on the pyramidal Cu cluster? ii) How does the electric field affect the above reaction?

Here, a CO molecule is first adsorbed on a pyramidal Cu cluster. Then, an O atom is introduced in the CO pre-adsorbed system. The nudged elastic band (NEB) method is applied to find out the transition state (TS), and then to determine the corresponding E_b and reaction energy E_r values. Electric fields with different orientations and intensities are superimposed to investigate the variations of the E_{ad} and E_b values. In addition, the field-induced geometric and electronic properties are further measured and analyzed. Our results demonstrate that the binding strength of CO/Cu clusters is twice as large as that of CO/Cu(111) surface while the field-induced E_b value is close to—or even lower than—that of commonly used catalytic surfaces, such as Rh(111), Pt(111), and Pd(111).

Calculations

All the DFT calculations are performed using the DMol³ code.^[60–61] The generalized gradient approximation (GGA) with Revised-Perdew–Burke–Ernzerhof (RPBE) functional^[62] is employed to describe exchange and correlation effects. A 0.002 Ha of smearing to the orbital occupation and 5.5 Å of global orbital cutoff radius are applied to achieve accurate electronic convergence. DFT Semi-core Pseudopotentials (DSPP) core treatment method is implemented for relativistic effects, which replaces core electrons by a single effective potential. The double numerical atomic orbital augmented by a polarization function (DNP) is chosen as the basis set. In addition, spin polarization is introduced since free Cu atoms contain one unpaired 4s electron.

A five-layer pyramidal Cu cluster containing 55 atoms is established with the symmetry of C_{4v} . As shown in Figure 1a, the four facets are equilateral triangle and the bottom facet is square. Each bond length d within the cluster is 2.56 Å, which equals the distance in a close-packed Cu (111) surface. In view of the fact that, experimentally, a pyramidal cluster cannot remain unattached but has to be placed on a substrate, the movement of the bottom layer will be restricted to some extent.^[63] Therefore, all atoms in our models are allowed to fully relax except the ones in the bottommost layer. The average $E_c = -2.33$ eV per atom for the cluster here is about 0.21 eV larger than that of the icosahedral Cu₅₅ cluster.^[47] Thus, the icosahedron is more stable than the pyramid for a given number of atoms. By estimating the dissociation energy of the uppermost vertex atom, our prior work has demonstrated that the tip of the five-layer pyramidal Cu cluster is quite stable.^[48] This agrees with the experimental result that a single-atom-ended nanopyramid is a thermodynamically stable structure during the heating process.^[64–65] For comparison purposes, the four-layer Cu(111) and twelve-layer Cu(211) surface systems are

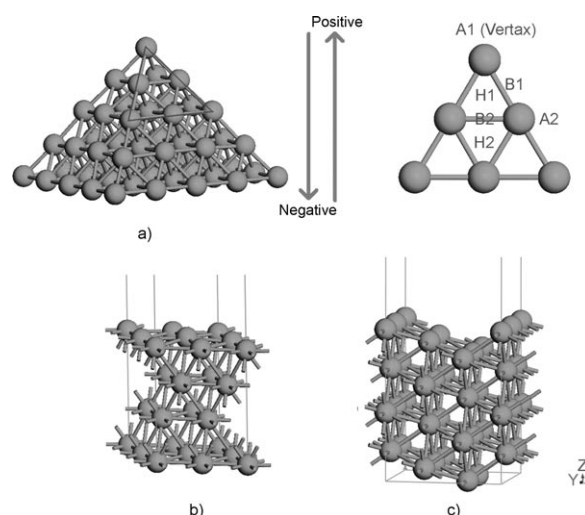


Figure 1. Schematic plots for the five-layer pyramidal Cu cluster (a), the flat Cu(111) surface (b), and the stepped Cu(211) surface (c). Six adsorption sites are labeled in plot (a), where A, B, and H indicate Atop, Bridge, and Hollow sites, respectively. The arrows indicate the direction of an electric field.

constructed with a vacuum width of 12 Å in the vertical direction, as seen in plots (b) and (c) of Figure 1. A (2×2) and (2×1) unit cell is set for the flat Cu(111) and stepped Cu(211) surface, respectively, with a $5 \times 5 \times 1$ k -point sampling. The bottom two layers are fixed in their calculated bulk positions, while the other layers are allowed to relax.

To facilitate comparison with previous published results,^[22,56] an O atom—not an O₂ molecule—is selected as a reactant in this study. Four steps are taken into account to describe the entire reaction: i) CO adsorption on a Cu cluster; ii) O-atom co-adsorption on the CO-pre-adsorbed Cu cluster; iii) CO reaction with O and formation of a nascent CO₂; and iv) release of the nascent CO₂ from the Cu substrate. In some studies an O₂ molecule was considered as a reactant, which renders a two-step mechanism: 1) $\text{CO} + \text{O}_2 \rightarrow \text{CO}_2 + \text{O}$ and 2) $\text{O} + \text{CO} \rightarrow \text{CO}_2$.^[44–46] Although our one-O system could be recognized as the second step of the above reaction, the reactant of atomic O may limit the present studies and leave out important reaction steps. To allow for a proper comparison we do not select reactions related to the O₂ molecule, but instead select the one having precisely the same $\text{O} + \text{CO} \rightarrow \text{CO}_2$ mechanism. Since we intend to clarify the size effect on the adsorption and the field effect on the reaction rate, a simpler process with only one O atom involved should be a better prototype.

A CO molecule is first placed on the Cu atom at the uppermost vertex of the pyramidal cluster.^[48] For Cu(111) and Cu(211) surfaces, CO is located at the atop site according to the experimental observation.^[52–54] The initial C–O distance is set to 1.13 Å in light of available experimental data.^[66] In this case, the E_{ad} value determined is the difference of the total amount of the considered system (E_t) and the corresponding cluster (E_{Cu}) and free gas (E_{CO}), namely, that $E_{ad} = E_t - E_{Cu} - E_{CO}$. Thereafter, three possible CO + O coadsorption configurations (Middle, Hollow, and Bridge sites) are established and depicted in plots (a)–(c) of Figure 2. In this case, $E_{ad} = E_t - E_{(Cu+CO)} - 1/2 E_{O_2}$,

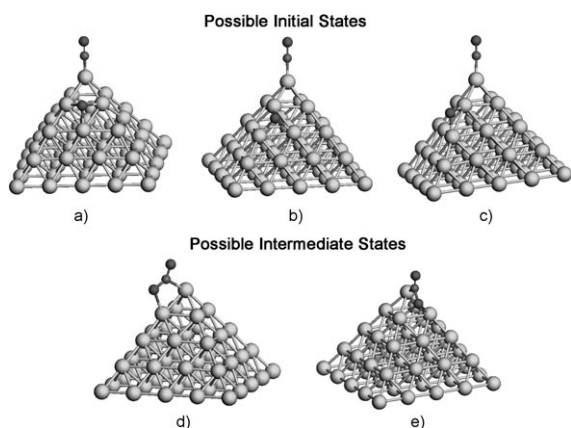


Figure 2. Three possible initial states for CO oxidation on a Cu cluster: a) Middle site, b) Hollow site, and c) Bridge site. Two possible intermediate states are depicted in (d) and (e), where the latter is proven to be unsuitable. The largest, smallest, and middle spheres represent Cu, C, and O atoms, respectively.

where the subscripts “Cu + CO” and “O₂” denote the pre-adsorbed system and the free O₂ molecule, respectively. Two *unrelaxed* intermediate structures are pre-established and shown in plots (d) and (e) of Figure 2. For the former, the nascent CO₂ locates on the bridge site at the ridge of the cluster. A new bond is created between CO and O, and both C and O participate in coordination with the cluster. Our calculations found that the relaxed O–C–O fragment still binds to the cluster with $d_{\text{C-Cu}}=2.042$ and $d_{\text{O-Cu}}=2.115$ Å. In the case of Figure 2e, the nascent CO₂ is located on the hollow position at the equilateral triangle facet of the cluster. The O atom also connects with CO but coordinates to two Cu atoms. It is worth pointing out that the above structure cannot be used as an intermediate state since the O–C–O fragment will desorb from the Cu cluster after relaxation. Therefore, the first transition state will be searched based on three initial states (as seen in Figure 2a–c) and the intermediate state depicted in Figure 2d.

The minimum energy paths (MEP) for CO oxidation and CO₂ desorption are determined using NEB method, which introduces a fictitious spring force that connects neighboring points on the path to ensure continuity of the path and projection of the force.^[67] The “Electric_Field” keyword in the DMol³ code allows us to specify the direction and intensity of an electric field. Homogeneous external electric fields will be introduced along the z axis in this work, where the upward and downward arrows in Figure 1 indicate the positive (+) and negative (–) field, respectively. The field intensities of $F=0.005$ and 0.010 au are chosen where 0.01 au corresponds to 5.14 V nm^{–1}.

2. Results and Discussion

The calculated E_{ad} values of the CO/Cu(111) surface, CO/Cu(211) surface, and CO/Cu cluster are shown in Table 1. To provide a comparison, available experimental^[52–54] and other theoretical results^[49–51,68–69] are also listed therein. Our calculated $E_{\text{ad}}=-0.48$ eV for the (2×2) CO/Cu(111) system agrees very well with available experiment results of $E_{\text{ad}}=-0.46$ to

Table 1. Computed adsorption energy E_{ad} , energy barrier E_{b} , and reaction energy E_{r} in eV for the CO adsorption and oxidation on Cu. The available experimental results $E_{\text{ad}1}$,^[52–54] and other simulation results $E_{\text{ad}2}$ ^[49–51,68–69] are also listed for a comparison purpose.

	Substrate	$-E_{\text{ad}}^{\text{[a]}}$	$-E_{\text{ad}1}$	$-E_{\text{ad}2}$
Adsorption	Cu(111)	0.48	0.46–0.52 ^[52–54]	0.42–0.46 ^{[49,51][b]} 0.62–0.90 ^{[50–51][c]}
	Cu(211)	0.69	0.61 ^[54]	0.68 ^{[68][b]} 0.86–0.96 ^{[68–69][c]}
	Cu cluster	0.72		
	Site	$-E_{\text{ad}}^{\text{[d]}}$	$-E_{\text{r}}$	E_{b}
Oxidation	Middle	1.38	0.535	1.317
	Hollow	1.73	0.182	1.759
	Bridge	1.41	0.509	1.471

[a] In the CO adsorption step, $E_{\text{ad}}=E_{\text{t}}-E_{\text{Cu}}-E_{\text{CO}}$. [b] Results from the GGA-RPBE functional. [c] Results from the GGA-PBE or GGA-PW91 functional. [d] In the O + CO coadsorption step, $E_{\text{ad}}=E_{\text{t}}-E_{\text{Cu+CO}}-1/2E_{\text{O}_2}$.

–0.52 eV^[52–54] which confirms the validity of our accuracy settings and calculation method. On the contrary, $E_{\text{ad}}=-0.62$ to -0.90 eV, obtained from GGA-PBE and PW91 functionals,^[50–51] are relatively lower than those from experiments^[52–54] and the RPBE functional.^[49,51] In our calculations, the magnitudes of E_{ad} are found to be -0.51 , -0.48 , and -0.06 eV, respectively, when a molecule is adsorbed on the (3×3), (2×2), and (2×1) Cu(111) surfaces at coverage rates of $\theta=0.11$, 0.25, and 0.50 monolayer (ML). The above results demonstrated that E_{ad} is quite sensitive to the CO coverage, and the binding strength decreases as the coverage increases. In comparison with the (111) surfaces of Pt, Rh, and Pd, the interaction between CO and the Cu(111) surface is very weak.^[49–50] In the case of (2×1) Cu(211) surface, our calculated $E_{\text{ad}}=-0.69$ eV is close to -0.61 eV obtained from the thermal desorption spectroscopy,^[54] and other theoretical data from RPBE functional.^[68] Therefore, the stepped surface has stronger adsorption ability than that of the flat surface.

In the case of the CO/Cu cluster, six different adsorption sites labeled in Figure 1a were examined to determine the most favorable structure. The calculated $-E_{\text{ad}}=0.72$, 0.69, 0.59, 0.35, 0.38, and 0.48 eV, respectively, at A1, A2, B1, B2, H1, and H2 sites. Therefore, the most stable adsorption site is the position on top of the uppermost vertex, that is, the A1 site. It is readily seen from Table 1 that the calculated E_{ad} value is dramatically lowered from -0.48 to -0.72 eV when a Cu cluster is utilized instead of the Cu(111) surface. This binding strength is even larger than that on the stepped Cu(211) surface. Thus, small pyramidal Cu clusters might be used as a catalyst for oxidation of the CO gas. When CO is adsorbed on a Cu cluster with relaxation depth of two layers (i.e. the bottom three layers are constrained), the calculated $E_{\text{ad}}=-0.68$ eV is -0.04 eV larger than that with relaxation depth of all but the bottom layer. This is presumably because fewer Cu atoms are allowed to relax in this case, which results in a higher free energy.

Thereafter, an O atom is adsorbed on a Cu atom with CO pre-adsorbed on a neighboring Cu atom. As listed in Table 1,

$E_{\text{ad}} = -1.38$, -1.73 , and -1.41 eV for the Middle, Hollow, and Bridge sites, respectively. It is discernable that the Hollow site location has the lowest E_{ad} value due to the longest distance between CO and O. All the three structures are considered as a reactant in our following oxidation calculations. Although several configurations of intermediate states are examined, only the structure in Figure 2d can stably exist on the Cu cluster. Otherwise, a CO_2 gas is spontaneously produced on the basis of the C–O–O fragment after relaxation. Noteworthy is the fact that our nascent CO_2 molecule [as seen in plot (d)] resembles that reported in the literature,^[70] investigating the CO oxidation on a Pt_{10} cluster. In that work, the most favored adsorption mode of the C–O–O fragment was also adsorbed on a bridge position at the ridge of the pyramidal cluster.

The calculated E_{b} values for the oxidation stage are 1.317, 1.759, and 1.471 eV for the Middle, Hollow, and Bridge sites, respectively, as shown in Figure 2. Therefore, the Middle site should be the most preferable initial state among the three candidates, which has the fastest reaction rate (with $E_{\text{b}} = 1.317$ eV) and the largest driven force (with $E_{\text{r}} = -0.535$ eV). The above oxidation pathway is described in detail in Figure 3.

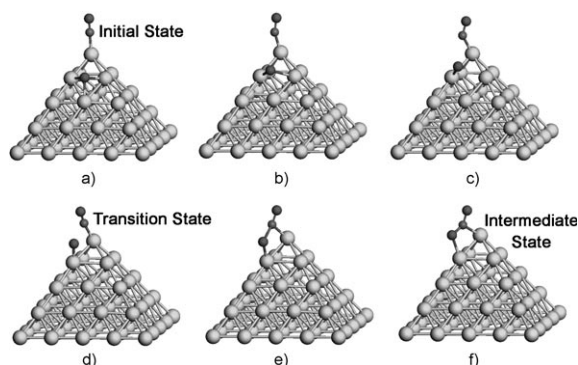


Figure 3. Snapshots of the minimum energy path (MEP) for CO oxidation on the Cu cluster. The largest, smallest, and middle spheres represent Cu, C, and O atoms, respectively.

As shown in plot (a), the CO molecule and the O atom are at their original positions at the very beginning of the reaction. Thereafter, CO rotates towards O and the first O–Cu bond breaks in plot (b), and then the second O–Cu bond also breaks in plot (c). Both CO and O move closer and closer to each other, and plot (d) shows the first transition state (TS1). Then in plot (e), the two adsorbates move so close that a new bond is formed between CO and O. The oxidation process is completed in plot (f), where the distance between the O and C atoms decreases, and a metastable O–C–O fragment (or a nascent CO_2) is finally produced.

Although the Cu cluster is able to oxidize the CO gas, its lowest $E_{\text{b}} = 1.317$ eV is much higher than those of the commonly used catalysts, merely around 1.000 eV.^[22] To lower the barrier, negative fields with different intensities are superimposed into the above reaction. Figure 4 shows the minimum reaction path in the presence of different field strengths, where the left and right parts indicate the oxidation and de-

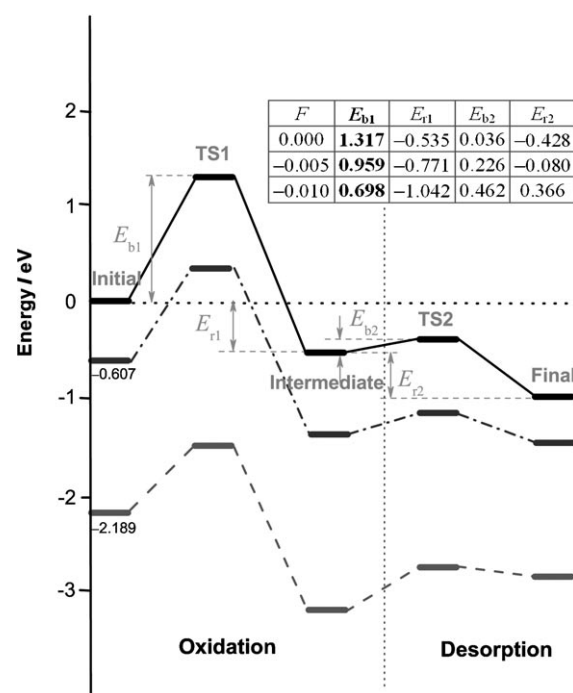


Figure 4. Relative energy plots in the presence of different electric fields, where the left (or right) part shows the oxidation stage (or the desorption stage). E_{b1} is defined as the energy of the TS1 minus that of the initial state, while E_{r1} is defined as the energy of the intermediate state minus that of the initial state. E_{b2} is defined as the energy of the TS2 minus that of the intermediate state, while E_{r2} is defined as the energy of the final state minus that of the intermediate state. The solid (—), dashed-dotted (---), and dashed (----) lines denote the results under 0.000, -0.005 , and -0.010 au fields, respectively.

sorption stages, respectively. It is worth noting that the intermediate state is a product in the oxidation stage (as seen in Figure 3 f), whereas a reactant is in the desorption stage (as seen in Figure 5a). In the absence of an electric field, the energy of the initial state is chosen as a reference and set to zero. Since the electric fields can apparently cause differences in energy, the energy reference states are lowered to -0.607 and -2.189 eV, respectively, in the presence of a -0.005 and -0.010 au field. It is readily seen that the barrier decreases

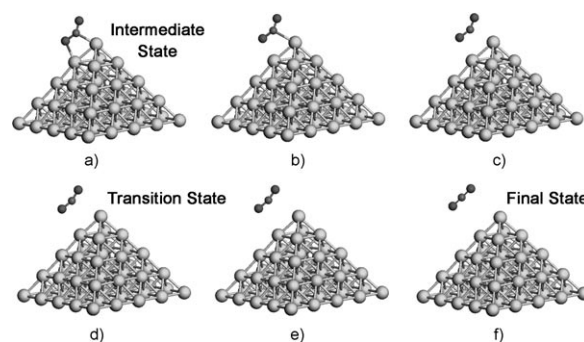


Figure 5. Snapshots of the minimum energy path (MEP) for nascent CO_2 desorption from the Cu cluster. The largest, smallest, and middle spheres represent Cu, C, and O atoms, respectively.

with increasing F , where the E_b value is lowered from 1.317 to 0.959 eV after superimposing a -0.005 au field; this value is lower than that of the usually used Rh(111) surface with $E_b = 1.17$ eV.^[22] The catalytic activity can thus be significantly enhanced due to the exponential relationship between the reaction rate and the E_b value.^[35] The barrier can be further lowered to 0.698 eV when $F = -0.010$ au, which is even less than $E_b = 0.79$ eV for Pt(111) and $E_b = 0.91$ eV for Pd(111) surfaces.^[22] Correspondingly, the reaction-driven force is also enhanced with increasing F , where $E_r = -0.535$, -0.771 , and -1.042 eV when $F = 0.000$, -0.005 , and -0.010 au, respectively. On the contrary, a positive field is apparently deleterious to the CO adsorption and oxidation. Regardless of $F = +0.002$, $+0.005$, or $+0.010$ au, the prebuilt O–C–O fragment becomes a CO₂ molecule and desorbs from the Cu cluster.

To understand the changes of the electronic structure in the presence of an electric field, Hirshfeld charge analysis was carried out for the Cu cluster, and the results are listed in Table 2.

Table 2. Hirshfeld charge analysis for the Cu cluster under $F = 0.000$, -0.010 , and $+0.010$ au, where the unit of the atom charge is one electron charge e . ^[a]				
Layer	Atom	$F = 0.000$ au	$F = -0.010$ au	$F = +0.010$ au
I	Cu(1)	+0.0095	-0.1998	+0.2014
	Cu(2)	-0.0020	-0.0655	+0.0610
II	Cu(3)	-0.0019	-0.0655	+0.0610
	Cu(4)	-0.0084	-0.0519	+0.0363
	Cu(5)	-0.0097	-0.0327	+0.0137
III	Cu(6)	-0.0084	-0.0519	+0.0363
	Cu(7)	+0.0090	-0.0155	+0.0342
	Cu(8)	-0.0092	-0.0204	+0.0027
	Cu(9)	-0.0092	-0.0204	+0.0027
IV	Cu(10)	+0.0090	-0.0155	+0.0342
	Cu(11)	+0.0188	+0.0725	-0.0357
	Cu(12)	-0.0085	+0.0328	-0.0488
	Cu(13)	-0.0082	+0.0302	-0.0465
	Cu(14)	-0.0085	+0.0328	-0.0488
V	Cu(15)	+0.0188	+0.0725	-0.0357

[a] The Cu atoms in this table are labeled in Figure 6a.

To provide a valid comparison, the results in the absence of an electric field are also listed in this table. In the case of the uppermost vertex, the charge carried by the Cu(1) atom decreases significantly from $+0.0095$ to -0.1998 e when a -0.010 au field is superimposed. Similarly, each atom in layers II to IV obtains charges and becomes anion in the presence of a negative field. However, Cu(11)–Cu(15) atoms in layer V lose electrons and become cations. This result demonstrates that charges move upward in the presence of a negative field. Therefore, the catalytic activity of the cluster can be improved since the charge transfer between the adsorbate and metal is enhanced. An opposite charge transfer direction can be achieved with a positive field. When $F = +0.010$ au, it is readily seen from this table that positive charges are presented from Cu(1) in layer I to Cu(10) in layer IV; whereas negative charges are presented from Cu(11) to Cu(15) in layer V. Since the upper four layers lose electrons whereas the bottommost layer accumulates

electrons, charges move downward in the presence of a positive field.

The field-induced changes in geometric structures were also measured for the Cu clusters. As shown in Figure 6a, the atomic distances d along the ridge of the cluster are 2.522,

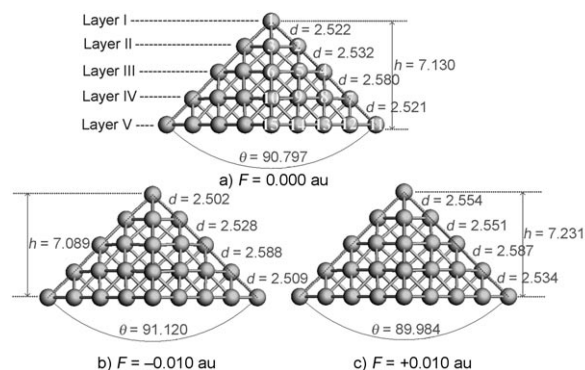


Figure 6. The geometric structure (height of the cluster h in Å, vertex angle θ in degree, and atomic distance d along the ridge of the cluster in Å) of the pyramidal Cu cluster under $F = 0.000$ (a), -0.010 (b), and $+0.010$ au (c).

2.532, 2.580, and 2.521 Å from layer I to layer V. These data are changed to 2.502, 2.528, 2.588, and 2.509 Å when $F = -0.010$ au, as seen in plot (b). Correspondingly, the height of the cluster h decreases from 7.130 to 7.089 Å and the vertex angle θ increases from 90.797° to 91.120° , which implies that a negative field compresses the cluster. The opposite conclusion can be achieved in the case of $F = +0.010$ au. As shown in plot (c), h increases from 7.130 to 7.231 Å and θ declines from 90.797° to 89.984° . These results confirm that a positive field elongates the cluster.

The final step is desorption of the nascent CO₂, where the intermediate state in Figure 5a becomes the reactant in this case. The newly formed O–C–O fragment is quite stable whereas the distance between O and Cu elongates and finally breaks in plot (b). Thereafter, the C–Cu bond also breaks in plot (c) and all direct connections between the O–C–O fragment and the Cu substrate disappear. The fragment continues to move away from the substrate, and plot (d) corresponds to the second transition state (TS2). The angle of the fragment α decreases gradually in the next few steps [see plot (e)], and finally, a free CO₂ molecule is produced with α approaches to 180° in plot (f). The NEB calculation finds that the desorption barrier is merely 0.036 eV in the absence of a field. However, the barrier increases with F increasing in the CO₂ desorption stage, where $E_b = 0.226$ and 0.462 eV when $F = -0.005$ and -0.010 au, respectively. As shown in the right part of Figure 4, the energy of final state is even larger than that of the intermediate state under -0.010 au field (with $E_{i2} = 0.366$ eV). This result implies that a strong intensity is bad for the CO purification since molecule desorption will be poor in this case. Since we have demonstrated that a positive field is helpful to the gas release, the ideal case for the CO purification might be: superimpose a negative field during the oxidation stage, whereas impose a positive field or just withdraw the field (since the E_b

value without the field is close to zero) during the desorption stage. However, noteworthy is the fact that although the oxidation can be accelerated whereas desorption can be decelerated by a negative field, the total barrier $E_b = 1.185$ eV at $F = -0.005$ au is still smaller than 1.353 eV in the absence of any field.

The geometric parameters for the entire series of reactions are measured and listed in Table 3, where "O1" and "O2" in the subscripts indicate the O atom in CO and the original free O

Table 3. Electric-field-induced geometric parameters (bond length d in Å and bond angle α of the O1–C–O2 fragment in degree) for the CO oxidation and CO₂ desorption on the Cu cluster.

F	Para. ^[a]	Initial	TS1	Intermediate	TS2	Final ^[c]
0.000 au	d_{O1-C}	1.145	1.156	1.208	1.190	1.170
	d_{C-Cu}	1.833	1.837	2.042	2.796	3.905
	d_{O2-Cu}	1.918 ^[b]	1.757	2.115	2.694	3.734
	d_{O2-C}	4.057	2.104	1.237	1.207	1.168
	α			141.806	160.685	179.497
–0.005 au	d_{O1-C}	1.158	1.124	1.222	1.212	1.183
	d_{C-Cu}	1.825	1.862	1.995	2.736	3.894
	d_{O2-Cu}	1.920	1.762	2.099	2.725	3.718
	d_{O2-C}	4.053	2.428	1.259	1.202	1.178
	α			134.515	151.198	177.764
–0.010 au	d_{O1-C}	1.175	1.168	1.238	1.205	1.177
	d_{C-Cu}	1.803	1.854	1.975	3.095	3.866
	d_{O2-Cu}	1.932	1.828	2.104	3.027	3.659
	d_{O2-C}	4.110	2.535	1.276	1.187	1.164
	α			129.362	154.512	174.465

[a] "O1" and "O2" indicate the original O atom in CO and the original free O atom, respectively. [b] The value between the O₂ atom and the Cu is an average of the three bond lengths. [c] Final state indicates that the CO₂ gas emits from Cu, and thus both the CO₂ and the Cu are free.

atom, respectively. All parameters listed in the table are related to the structures in Figures 3 and 5. In the absence of a field, on one hand, the bond length between O1 and C (d_{O1-C}) increases from 1.145 Å in the initial state to 1.156 Å in TS1, and then to 1.208 Å in the intermediate state. This result can be attributed to the weakness of the binding between O1 and C in the oxidation stage. On the other hand, d_{O1-C} decreases to 1.190 Å and finally to 1.170 Å in TS2 and the final state during the desorption stage. Different from d_{O1-C} , d_{C-Cu} continuously increases in the entire process due to the formation of the O2–Cu bond as well as the release of CO₂ gas. The bond length between O2 and Cu d_{O2-Cu} first increases from 1.918 to 2.115 Å since the newly formed O2–C bond in the intermediate state weakens the interaction between O2 and Cu. Thereafter, d_{O2-Cu} increases to 2.694 and 3.734 Å due to the release of the CO₂ molecule. In contrast, the distance between O2 and C, d_{O2-C} maintains decreasing from 4.057 to 1.168 Å. α denotes the angle of the O1–C–O2 fragment, which increases from 141.806° in the intermediate state to 179.497° in the final state. Since the latter is very close to 180°, a "free" CO₂ gas is thus produced.

It is discernable from Table 3 that the presence of a negative field causes evident changes in geometric parameters. However, similar variation trends are found for each parameter during

the entire reaction in comparison with those in the absence of a field. For example, d_{O1-C} under $F = -0.005$ au also increases from 1.158 Å in the initial state to 1.222 Å in the intermediate state, and then decreases to 1.183 Å in the final state. In this case, the d_{O1-C} values are slightly larger than those without a field, because a negative field enhances the binding strength between C and Cu, and thus weakens that between O1 and C. d_{C-Cu} in the initial state decreases from 1.833, 1.825, to 1.803 Å when F changes from 0.000, –0.005, to –0.010 au, which is consistent with a prior conclusion that the binding strength of CO increases toward negative fields.^[57] This trend can be further confirmed by our calculated $E_{ad}(F)$ values for CO on the pyramidal Cu cluster, where $E_{ad} = -0.72, -0.77, -0.99$ eV when $F = 0.000, -0.005$ and -0.010 au, respectively. On the contrary, d_{O2-Cu} increases as F increases. For example, in the initial state, $d_{O2-Cu} = 1.918, 1.920, \text{ and } 1.932$ Å when $F = 0.000, -0.005, \text{ and } -0.010$ au, respectively. The distance between the released CO₂ and Cu (d_{C-Cu} and d_{O2-Cu} in the final state) is shortened when F increases. In addition, α in the final state decreases gradually from 179.497° to 174.465° if F increases from 0.000 to –0.010 au. These phenomena suggest that in the latter case the physisorption between the CO₂ gas and the substrate is stronger than that in the absence of a field. In the oxidation stage, our d_{O2-C} in TS1 increases while E_b decreases with F increasing from 0.000, –0.005, to –0.010 au. In the desorption stage, however, d_{O2-C} in TS2 decreases while E_b increases with increasing F , which agrees with a prior conclusion that the shorter the d_{O2-C} is at the TS, the higher the barrier.^[22]

Blyholder's model states that one lone electron pair is donated from the nonbonding CO-5 σ orbital into empty metal orbitals, and back-donated from occupied metal d orbitals to empty CO-2 π^* orbital, simultaneously.^[71] Thus, the variation in bond strength is caused by 2 π^* –d coupling; namely, the stronger this coupling, the stronger the CO–metal bonding.^[72] Under a negative field, the electrons are moved upward and thus more charges can participate in the transfer between Cu and CO. To look into the field-induced spin states, spin partial density of state (PDOS) is obtained for the Cu cluster and shown in Figure 7. Both spin-up (α) and spin-down (β) densities are given in the presence of 0.000, –0.005, and –0.010 au fields. In the absence of any electric field, the band of the cluster is dominated by the d orbital. Large contributions from s and p orbitals can be detected in plot (a), and the p state becomes especially intensive for the orbitals above the Fermi level. It is readily seen from the plot that β is identical with α except the direction. In comparison with plot (a), the main peak of the d state moves from –1.84 to –0.34 when a –0.005 au field is superimposed; and then shifts to 0.38 eV when the field is further enhanced to –0.010 au. Although all the bands are pushed toward the Fermi level by the negative fields, large spd hybridization can also be observed in the spin PDOS, as seen in plots (b) and (c). Moreover, the shapes of α and β PDOS of the s, p, and d states are still perfectly matching, indicating its zero magnetic moment.

To further understand the electronic hybridization behavior, the PDOS charts are determined and depicted in Figure 8. The intermediate state is chosen as an example here since its struc-

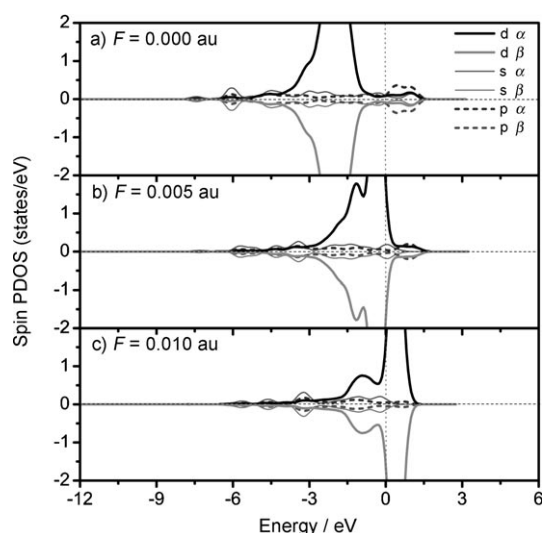


Figure 7. Spin PDOS plots of the pyramidal Cu cluster under $F=0.000$ (a), -0.005 au (b), and -0.010 au (c). Spin-up (α) and spin-down (β) states are given in each case. The Fermi level is set to zero and indicated by a dashed line.

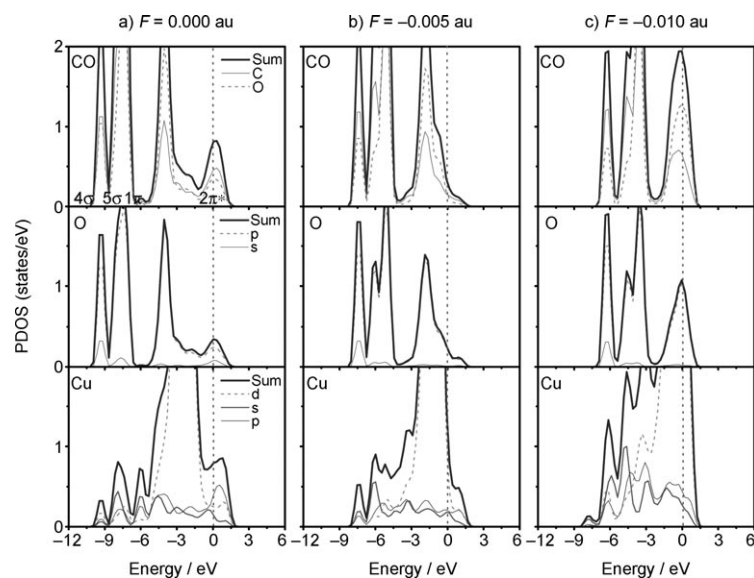


Figure 8. PDOS plots for the intermediate state under $F=0.000$ (a), -0.005 (b), and -0.010 au (c). The Fermi level is set to zero and indicated by a dashed line.

ture and energy are essential parameters in the catalytic oxidation studies. We first address the hybridization conditions for the system in the absence of an electric field. In the CO side, the CO- 4σ orbital is localized at -9.34 eV after adsorption. Both CO- 5σ and CO- 1π orbitals broaden and dominate the interaction, where the 5σ orbital shifts even below the 1π orbital. The initial empty antibonding CO- $2\pi^*$ orbital is pulled below the Fermi level, which is partially populated due to back-donation of d electrons and the electronic resonance.^[46] It can be seen that the accumulation of charge density for the CO- 5σ orbital is around the C atom, whereas that for the CO- $2\pi^*$ orbital below the Fermi level is around the O atom. Corre-

spondingly, two new peaks composed of the $2s+2p$ of O, and $3d+4s$ of Cu appear at the lower energy range and hybridize with the CO- 4σ orbital at -9.34 eV. All the peaks of the O atom overlap exactly with those of the CO molecule, which confirms the formation of the chemical bond between CO and O in the intermediate state. The result for the O atom shows that all the bands are due to almost exclusively O- $2p$ electrons, with a small degree of hybridized O- $2s$ states at the lowest energy range. In the higher energy range, Cu- $3d$, Cu- $4s$, and even Cu- $4p$ orbitals overlap with the CO- 5σ and CO- 1π orbitals at -8.17 and -7.43 eV, respectively.

It is readily seen from Figure 8 that the PDOS plots in the presence of a negative field are quite similar to those without a field, although all the bands are pushed toward the Fermi level. When $F=-0.005$ au, the peak of CO- 4σ interacts with those of Cu and O at -7.34 eV. The CO- 5σ and 1π orbitals still broaden and located at -5.93 and -5.21 eV, respectively. In this case, the bands of Cu and O also move to the higher energy range and overlap with each other. If the band without a field is selected as a reference, it is readily seen that all the bands are further shifted towards the Fermi level after super-

imposing a -0.010 au field. For example, the sharpest peak of CO moves significantly from -5.21 to -3.61 eV when F increases from -0.005 to -0.010 au. In all cases, these peaks continue to be hybridized strongly with those of Cu and O. This orbital hybridization confirms the existence of the nascent CO₂ fragment above the Cu cluster, and the strong interactions between the adsorbate and the substrate, even in the presence of electric fields. Since the $2\pi^*-d$ coupling increases as the d -band center shifted toward the Fermi level,^[73] the PDOS plots illustrate again that the reaction activity of the Cu cluster can be significantly enhanced after superimposing a negative field.

In light of the above discussion, it is evident that the adsorption behavior and catalytic reaction can be influenced by an external electric field. In a recent work, division of voltage (for 3 V) by tip-sample distance (ca. 5 Å), a field of about $0.6 \text{ V}\text{\AA}^{-1}$, which is about 0.012 au, was achieved in experiments.^[58] Noteworthy is the fact that this value is even larger than the strongest intensity ($F=0.010$ au) used herein. Considering the facts that the tip-sample distance could be further lowered with the advent of

modern developments in nanofabrication, the required field intensity could be further enhanced and readily attained in a practical system.

3. Conclusions

In conclusion, DFT calculations with electric fields were carried out to study the catalytic oxidation reaction of CO on a pyramidal Cu cluster. The binding strength of the CO/Cu cluster was found to be twice as strong as that of the CO/Cu(111) surface. The metastable O-C-O fragment could be formed on the Cu cluster, and the oxidation barrier was significantly lowered

from 1.317, 0.959, to 0.698 eV when F increased from 0.000, -0.005 , to -0.010 au. No energy barrier existed for the CO_2 release when a positive field was superimposed. The enhanced reaction activity is attributed to the charge redistribution induced by an electric field.

Acknowledgements

W. Liu, R. Q. Zhang, and Q. Jiang acknowledge financial support from the National Key Basic Research and Development Program of China (Grant No. 2004CB619301, 2010CB631001). Y. H. Zhao, Y. Li, and E. J. Lavernia would like to acknowledge support by the Office of Naval Research of the USA (Grant No. N00014-08-1-0405) with Dr. Lawrence Kabacoff as program officer.

Keywords: adsorption · catalytic oxidation · density functional calculations · external electric field · nanoclusters

- [1] Y. Nishihata, J. Mizuki, T. Akao, H. Tanaka, M. Uenishi, M. Kimura, T. Okamoto, N. Hamada, *Nature* **2002**, *418*, 164–167.
- [2] S. E. Mason, I. Grinberg, A. M. Rappe, *J. Phys. Chem. C* **2008**, *112*, 1963–1966.
- [3] T. Yamanaka, T. Matsushima, *Phys. Rev. Lett.* **2008**, *100*, 026104.
- [4] K. Kunimatsu, T. Sato, H. Uchida, M. Watanabe, *Langmuir* **2008**, *24*, 3590–3601.
- [5] C. Q. Sun, *Prog. Mater. Sci.* **2003**, *48*, 521–685.
- [6] P. J. Feibelman, B. Hammer, J. K. Norskov, F. Wagner, M. Scheffler, R. Stumpf, R. Watwe, J. Dumesic, *J. Phys. Chem. B* **2001**, *105*, 4018.
- [7] Y. Wang, S. de Gironcoli, N. S. Hush, J. R. Reimers, *J. Am. Chem. Soc.* **2007**, *129*, 10402–10407.
- [8] I. Dabo, A. Wieckowski, N. Marzari, *J. Am. Chem. Soc.* **2007**, *129*, 11045–11052.
- [9] Q. M. Hu, K. Reuter, M. Scheffler, *Phys. Rev. Lett.* **2007**, *98*, 176103.
- [10] M. Rieger, J. Rogal, K. Reuter, *Phys. Rev. Lett.* **2008**, *100*, 016105.
- [11] K. Reuter, M. Scheffler, *Phys. Rev. B* **2006**, *73*, 045433.
- [12] H. Orita, N. Itoh, Y. Inada, *Chem. Phys. Lett.* **2004**, *384*, 271–276.
- [13] P. Gruene, A. Fielicke, G. Meijer, D. M. Rayner, *Phys. Chem. Chem. Phys.* **2008**, *10*, 6144–6149.
- [14] W. Liu, Y. F. Zhu, J. S. Lian, Q. Jiang, *J. Phys. Chem. C* **2007**, *111*, 1005–1009.
- [15] P. H. T. Philipsen, E. vanLenthe, J. G. Snijders, E. J. Baerends, *Phys. Rev. B* **1997**, *56*, 13556–13562.
- [16] X. Ren, P. Rinke, M. Scheffler, *Phys. Rev. B* **2009**, *80*, 045402.
- [17] K. Doll, *Surf. Sci.* **2004**, *573*, 464–473.
- [18] G. Kresse, A. Gil, P. Sautet, *Phys. Rev. B* **2003**, *68*, 073401.
- [19] D. O. Scanlon, N. M. Galea, B. J. Morgan, G. W. Watson, *J. Phys. Chem. C* **2009**, *113*, 11095–11103.
- [20] M. Huang, S. Fabris, *J. Phys. Chem. C* **2008**, *112*, 8643–8648.
- [21] M. Gajdos, J. Hafner, *Surf. Sci.* **2005**, *590*, 117–126.
- [22] X. Q. Gong, Z. P. Liu, R. Raval, P. Hu, *J. Am. Chem. Soc.* **2004**, *126*, 8–9.
- [23] M. D. Ackermann, T. M. Pedersen, B. L. M. Hendriksen, O. Robach, S. C. Bobaru, I. Popa, C. Quiros, H. Kim, B. Hammer, S. Ferrer, J. W. M. Frenken, *Phys. Rev. Lett.* **2005**, *95*, 255505.
- [24] T. Yamanaka, *J. Chem. Phys.* **2008**, *128*, 171102.
- [25] G. Krenn, I. Bako, R. Schennach, *J. Chem. Phys.* **2006**, *124*, 144703.
- [26] S. Schwegmann, H. Over, V. DeRenzi, G. Ertl, *Surf. Sci.* **1997**, *375*, 91–106.
- [27] P. Boarini, V. Carassiti, A. Maldotti, R. Amadelli, *Langmuir* **1998**, *14*, 2080–2085.
- [28] C. B. Almquist, P. Biswas, *Appl. Catal. A* **2001**, *214*, 259–271.
- [29] E. D. German, M. Sheintuch, *J. Phys. Chem. C* **2008**, *112*, 14377–14384.
- [30] J. M. H. Lo, T. Ziegler, *J. Phys. Chem. C* **2008**, *112*, 3692–3700.
- [31] A. Cupolillo, G. Chiarello, V. Formoso, D. Pacile, M. Papagno, F. Veltri, E. Colavita, L. Papagno, *Phys. Rev. B* **2002**, *66*, 233407.
- [32] I. Nakai, H. Kondoh, K. Amemiya, M. Nagasaka, A. Nambu, T. Shimada, T. Ohta, *J. Chem. Phys.* **2004**, *121*, 5035–5038.
- [33] I. Nakai, H. Kondoh, T. Shimada, A. Resta, J. N. Andersen, T. Ohta, *J. Chem. Phys.* **2006**, *124*, 224712.
- [34] W. H. Chen, I. Ermanoski, T. Jacob, T. E. Madey, *Langmuir* **2006**, *22*, 3166–3173.
- [35] A. Alavi, P. J. Hu, T. Deutsch, P. L. Silvestrelli, J. Hutter, *Phys. Rev. Lett.* **1998**, *80*, 3650–3653.
- [36] A. Eichler, *Surf. Sci.* **2002**, *498*, 314–320.
- [37] S. Y. Liem, J. H. R. Clarke, *J. Chem. Phys.* **2004**, *121*, 4339–4345.
- [38] K. Bleakley, P. Hu, *J. Am. Chem. Soc.* **1999**, *121*, 7644–7652.
- [39] C. J. Zhang, P. Hu, *J. Am. Chem. Soc.* **2001**, *123*, 1166–1172.
- [40] Y. Gao, N. Shao, S. Bulusu, X. C. Zeng, *J. Phys. Chem. C* **2008**, *112*, 8234–8238.
- [41] C. Dupont, D. Loffreda, F. Delbecq, F. Aires, E. Ehret, Y. Jugnet, *J. Phys. Chem. C* **2008**, *112*, 10862–10867.
- [42] X. Y. Liu, A. Q. Wang, X. D. Wang, C. Y. Mou, T. Zhang, *Chem. Commun.* **2008**, 3187–3189.
- [43] L. M. Molina, B. Hammer, *Phys. Rev. Lett.* **2003**, *90*, 206102.
- [44] C. M. Chang, C. Cheng, C. M. Wei, *J. Chem. Phys.* **2008**, *128*, 124710.
- [45] L. M. Molina, B. Hammer, *J. Catal.* **2005**, *233*, 399–404.
- [46] W. An, Y. Pei, X. C. Zeng, *Nano Lett.* **2008**, *8*, 195–202.
- [47] W. Liu, D. Liu, W. T. Zheng, Q. Jiang, *J. Phys. Chem. C* **2008**, *112*, 18840–18845.
- [48] W. Liu, Y. H. Zhao, E. J. Lavernia, Q. Jiang, *J. Phys. Chem. C* **2008**, *112*, 7672–7677.
- [49] M. Gajdos, A. Eichler, J. Hafner, *J. Phys. Condens. Matter* **2004**, *16*, 1141–1164.
- [50] S. E. Mason, I. Grinberg, A. M. Rappe, *Phys. Rev. B* **2004**, *69*, 161401.
- [51] N. Lopez, J. K. Norskov, *Surf. Sci.* **2001**, *477*, 59–75.
- [52] P. Hollins, J. Pritchard, *Surf. Sci.* **1979**, *89*, 486–495.
- [53] W. Kirstein, B. Kruger, F. Thieme, *Surf. Sci.* **1986**, *176*, 505–529.
- [54] S. Vollmer, G. Witte, C. Woll, *Catal. Lett.* **2001**, *77*, 97–101.
- [55] C. J. Zhang, R. J. Baxter, P. Hu, A. Alavi, M. H. Lee, *J. Chem. Phys.* **2001**, *115*, 5272–5277.
- [56] S. Kandoi, A. A. Gokhale, L. C. Grabow, J. A. Dumesic, M. Mavrikakis, *Catal. Lett.* **2004**, *93*, 93–100.
- [57] S. A. Wasileski, M. T. M. Koper, M. J. Weaver, *J. Phys. Chem. B* **2001**, *105*, 3518–3530.
- [58] T. Mitsui, E. Fomin, D. F. Ogletree, M. Salmeron, A. U. Nilekar, M. Mavrikakis, *Angew. Chem.* **2007**, *119*, 5859–5863; *Angew. Chem. Int. Ed.* **2007**, *46*, 5757–5761.
- [59] M. Tomonari, O. Sugino, *Chem. Phys. Lett.* **2007**, *437*, 170–175.
- [60] B. Delley, *J. Chem. Phys.* **1990**, *92*, 508–517.
- [61] B. Delley, *J. Chem. Phys.* **2000**, *113*, 7756–7764.
- [62] B. Hammer, L. B. Hansen, J. K. Norskov, *Phys. Rev. B* **1999**, *59*, 7413–7421.
- [63] H. S. Kuo, I. S. Hwang, T. Y. Fu, J. Y. Wu, C. C. Chang, T. T. Tsong, *Nano Lett.* **2004**, *4*, 2379–2382.
- [64] T. Y. Fu, L. C. Cheng, C. H. Nien, T. T. Tsong, *Phys. Rev. B* **2001**, *64*, 113401.
- [65] T. Ishikawa, T. Urata, B. Cho, E. Rokuta, C. Oshima, Y. Terui, H. Saito, A. Yonezawa, T. T. Tsong, *Appl. Phys. Lett.* **2007**, *90*, 143120.
- [66] *CRC Handbook of Chemistry and Physics, 81th ed.* (Ed.: D. R. Lide), CRC, Boca Raton, **2000**.
- [67] A. Ulitsky, R. Elber, *J. Chem. Phys.* **1990**, *92*, 1510–1511.
- [68] M. Gajdos, A. Eichler, J. Hafner, G. Meyer, K. H. Rieder, *Phys. Rev. B* **2005**, *71*, 035402.
- [69] F. Mehmood, A. Kara, T. S. Rahman, K. P. Bohnen, *Phys. Rev. B* **2006**, *74*, 155439.
- [70] A. Eichler, *Phys. Rev. B* **2005**, *71*, 125418.
- [71] G. Blyholder, *J. Phys. Chem.* **1964**, *68*, 2772.
- [72] P. Crawford, P. Hu, *J. Phys. Chem. B* **2006**, *110*, 24929–24935.
- [73] B. Hammer, O. H. Nielsen, J. K. Norskov, *Catal. Lett.* **1997**, *46*, 31–35.

Received: June 4, 2009

Revised: August 27, 2009

Published online on November 10, 2009